FABRICATION AND TESTING OF A DROPLET-BASED MICROFLUIDIC NEURAL IMPLANT

Michael Minh-Hung Nguyen

Masters of Research
in the Department of Engineering

Department of Engineering
Macquarie University

December, 22 2014
Amended from 1st version published: 10th October 2014

Supervisor: Dr. David Inglis

Contents

List of Figures

List of Tables

ABSTRACT

Neuroscientists have used fine gauge electrodes to record and stimulate the brain for decades. The main problem is the majority of neurological disorders involve problems with the chemical neurotransmitters, not electrical or electrochemical signal transduction. Due to this, a localised method needs to be developed to treat neurochemical disorders.

This project investigates the fabrication of microfluidic device to be a chemical analogue to deep brain stimulation. We propose a modification to conventional droplet microfluidics that may enable water-based drug delivery and fluid sampling from the end of a microfabricated needle. The device will consist of a T-junction to generate water-in-oil droplets, a descending channel, a u-bend and a return channel. At the u-bend, the tip of the needle, a hydrophilic membrane will form the lid. Under positive/negative fluid pressure, droplets may be expelled/extracted through the membrane.

This thesis describes how the microfluidic needle was fabricated using hot embossing, which involves pressing a PDMS mould (fabricated from a PMMA master mould) into a COC substrate. This microfluidic needle was tested using the Maesflowregistered system to see if the channel is capable in producing water droplets in a continuous oil flow using a T-junction channel configuration. Bonding methods for bonding two COC substrates together, and a membrane to a COC lid were found in order to bond a COC lid to the embossed microfluidic channel.

STATEMENT OF CANDIDATE

I, Michael Minh-Hung Nguyen, declare that this report, submitted as part of the requirement for the award of Masters of Research in the Department of Engineering, Macquarie University, is entirely my own work unless otherwise referenced or acknowledged. This document has not been submitted for qualification or assessment an any academic institution.

Student's Name: Michael Minh-Hung Nguyen

Student's Signature:

Date: 22nd December 2014

ACKNOWLEDGMENTS

I would like to acknowledge Dr. David Inglis, Dr. Luke Parkinson, Ben Johnston, and Dr. Oya Sevimli. Dr. David Inglis has been my supervisor for the entire project and has greatly helped by providing personal support and training. He has also assisted with reviewing this thesis for submission. Dr. Luke Parkinson is a micorfluidics engineer at the University of South Australia. He has helped by fabricating the master PMMA moulds and providing ideas for fabricating more devices using the hot embossing method.

Ben Johnston is a laser applications engineer in the Department of Physics and Astronomy at Macquarie University, who was helped laser cutting the hydrophilic membranes for the needle. Dr. Oya Sevimli is a research fellow in the Department of Engineering at Macquarie University who suggested the Tresky bonding machine, which can be of great use to the project.

Chapter 1

Introduction

Various novel biomedical devices had been developed recently for medical diagnosis, therapy and drug delivery. The main outcomes of these therapeutic devices are improvements on the current medical methods being used in hospitals and in outpatients. These devices have developed new ways of delivering prescribed drugs to patients, using novel implants that increases the quality of life for patients.

1.1 Current Developments

1.1.1 Needles and Implants

Inspiration for implants can come from unexpected sources, for example, the Defense Advanced Research Projects Agency (DARPA), which is branch of the U.S. Department of Defense, is developing a program called Electrical Prescriptions, or ElectRx [20] that takes its inspiration from comic book superheroes and their superpowers to heal themselves. This device will monitor the body's organs, sensing any injuries or infections, and healing them when necessary. It sends electric impulses from the device to stimulate nerve patterns that are used to help the body heal itself, and stabilises the peripheral nervous system (which monitors the status of internal organs and regulate the bodys responses to infection and disease in a biological process called neuromodulation) from performing adverse effects such as exacerbate a condition.

Other medical implants that have been developed include microneedle patches for flu vaccination [19, 33], bionic eye implants [30], an integrated implant that controls a

brains neural network using light (known as optogenetics) [21], an eye sensor (specifically for glaucoma patients) [23], and a neural stimulation method that provides mild electrical stimulation to the brain via an implanted electrode called deep brain stimulation (DBS) [18].

1.1.2 Drug Delivery Systems

In another example using novel materials, researchers have created a drug delivery method that is triggered by an integrated system that monitors the patient's muscle movement [22], which will then decide when to deliver the drug that is preloaded into the system. It aims to treat Parkinson's disease and epilepsy. A collaborative effort by researchers from Seoul National University, University of Texas, health-monitoring device maker MC10 produced this electronic skin patch that contains the sensors, memory, and drug delivery components, which are made using semi-conductor fabrication processes and include nano-materials.

Intra muscular injections, like the flu vaccine, is another application where a patch is used as a medium for drug delivery. Traditional flu vaccinations [19] requires a patient to travel to their doctor and be injected with a long metal needle. It was commonly known that these injections are painful, especially to children. The vaccination patch was developed in a way that the drug delivery was less painful to the patient, while still administering the required dose. Each patch had fifty etched microneedles made of stainless steel, with a snap mechanism, using polypropylene screw caps to indicate a successful application. The patches were given to a sample of patients to try (with and without a supervisor) and the results show that more people would rather use the microneedle patches instead of a traditional injection. The effectiveness of the patch was measured by applying fluorescein to the patients skin after applying the flu patch, imaging it under blue LED light and counting the insertion sites. Tests show that the median number of insertion sites counted on the first attempt was 96%.

There has been developments for applying microfluidic systems into drug delivery, such as a localised microfluidic dispensing system to cellular networks, developed by Kraus *et al* [14]. It involves eight channels for drug delivery that travels into a main cell cultivation chamber at different specific regions of cells. The device was created using multiple layers made out of multiple materials such as: PDMS, Pyrex, and Silicon, which is designed to be integrated with a complementary metal oxide semiconductor.

1.2 Research Question

For decades, neuroscientists have used fine gauge electrodes to record and stimulate brain activity. Background information on brain activity shows that nerves transmit information within themselves electrically and cell-to-cell communication is transmitted chemically. Conventional brain implants focus on applying an electrical stimulation to the nerve cells and the nervous system. For example, a method that involves tiny electrodes implanted into a patients brain (which are powered by battery packs sewn into their chests) delivers a weak but constant electrical current which aims to reduce or eliminate symptoms of neurological disorders [18].

The main problem is the majority of neurological disorders involve problems with the chemical neurotransmitters, not electrical or electrochemical signal transduction. When treating these disorders, the standard method is to treat the whole patient and the whole brain with medication. However, neurochemical disorders are typically localised, similarly to neuroelectrical disorders, which means a localised method needs to be developed to treat neurochemical disorders.

1.2.1 Project Outcomes

Localising neurochemical disorder treatment requires fabricating a device that has the functionality of delivering drugs directly to affected areas of the brain. To achieve this, the device must deliver drugs with high spatial, temporal, and chemical resolution. Spatial resolution means controlling drug delivery locations with sub hundred micron precision. For the device to achieve temporal resolution, the device must be able to administer droplets with hundred microsecond on-off times. Chemical resolution is achieved when the device is able to administer multiple different drugs and doses within the same needle.

For some treatments, multiple drugs may need to be delivered to the same place (an exciter and a scavenger, for example). However, traditional drug delivery methods involve inserting a needle to the target area, delivering one drug through the needle, and removing the needle for the secondary drug to be delivered, to prevent contamination between different medicines.

Other conventional drug delivery methods include dialysis membranes, dialysis microtubing, and nano-pipettes. Dialysis membranes allow a single drug to be delivered to a cubic millimetre-size region. A dialysis microtube improves spatial resolution, however, not the temporal resolution. Nano-pipettes improves the spatial resolution further, however, the temporal resolution is still limited due to diffusion at the tip of the pipette.

To address these problems, a modification of Chen *et al*'s chemistrode [6] is pro-

posed. The chemistrode is a droplet-based microfluidic device that manipulates and records molecular signals with high spatial and temporal resolution. The operation of the chemistrode involve capturing molecular signals in aqueous droplets through coalescence, which are surrounded by a fluorocarbon carrier fluid. The device was fabricated by using rapid prototyping in poly(dimethyl siloxane) (PDMS).

The proposed device will be able to deliver drugs or sample extra cellular fluid using droplet-based microfluidics where aqueous droplets are entrained in a continuously flowing oil-phase. Further development of the microfluidic channel will allow the delivery of two or more drugs into the same oil-phase with high temporal resolution (less than one second), without the problem of contamination between different drugs. The needle will contain a return and outgoing port for the continuous oil phase. The tip of the needle will contain a sub-micron pore-sized, hydrophilic membrane in which the oil-phase will not pass through.

This project involves fabricating a prototype microfluidic neural implant into a thermoplastic substrate, and proving the conceptual idea of delivering water droplets through the hydrophilic membrane. Other major outcomes include designing the microfluidic master mould and embossing the device pattern into a thermoplastic base. Fabrication of the designed microfluidic channel requires collaboration with the Australian National Fabrication Facility at the University of South Australia (ANFF-SA).

Chapter 2

Theory

The laws governing microfluidic flows are the same as those in classical fluid dynamics. Fluid dynamics is the study of the motion of fluids, whether they are in liquid or gaseous form. The Eulerian assumption in fluid dynamics is that in any small volume of fluid, the system is still considered to be macroscopic, since there are still a great number of molecules within this volume. Hence any fluid is considered as a continuous system. Although microfluidic systems operate on a much smaller scale compared to traditional fluidic systems, the theory from fluid dynamics can still be used. Much to our benefit, this scale allows a number of simplifications, including incompressibility. The following sections starts with the most general equation, the Navier-Stokes Equation. It then explores the Reynolds number, viscosity, and the much simpler Stokes equation.

2.1 Navier-Stokes Equation

In order to theoretically illustrate the behaviour of a fluid flow, a mathematical solution is derived. This specific equation is called the Navier-Stokes equation. The Navier-Stokes equation comes from the general equation of motion for a viscous fluid, which encompasses the rate of change in momentum due to: convection of momentum, pressure forces, viscous forces, and body forces. [4].

In the text *"Theoretical Microfluidics"* [4], a worked proof via mathematical reasoning is shown, resulting in an equation that is known as the Navier-Stokes equation for Newtonian fluids:

$$\rho[\delta_t \boldsymbol{v} + (\boldsymbol{v} \cdot \nabla)\boldsymbol{v}] = -\nabla p + \eta \nabla^2 \boldsymbol{v} + \beta\eta\nabla(\nabla \cdot \boldsymbol{v}) + \rho \boldsymbol{g} + \rho_{el}\boldsymbol{E} \tag{2.1}$$

Where:

- ρ is density

- $\boldsymbol{v}$ is the velocity vector
- p is pressure
- η is the dynamic viscosity (internal friction due to sheer stress)
- β is a dimensionless viscosity ratio
  - Where $\beta \equiv \frac{\xi}{\eta} + \frac{1}{3}$, ξ is another viscosity value (internal friction due to compression)
- $\boldsymbol{g}$ is the acceleration of gravity
- $\rho_{el}\mathbf{E}$ is the electrical force in terms of the charge density ρ_{el} and the external electric field $\boldsymbol{E}$

The project uses water as the main fluid body, however the compressibility of water is very small (approximately $10^{-10}\ \frac{\nabla V}{V}/Pa$), meaning a dynamic or static pressure of 1 MPa of water results in a 0.01% change in volume. Because of this, fluids inside microfluidic systems can be treated as incompressible, which eliminates the dimensionless viscosity ratio β. This gives the following Navier-Stokes equation, including body forces:

$$\rho[\delta_t \boldsymbol{v} + (\mathbf{v} \cdot \nabla)\boldsymbol{v}] = -\nabla p + \eta\nabla^2\boldsymbol{v} + \rho\boldsymbol{g} + \rho_{el}\boldsymbol{E} \tag{2.2}$$

For excluding body forces (without gravity and external forces (such as electrical force) [4]):

$$\rho[\delta_t \boldsymbol{v} + (\boldsymbol{v} \cdot \nabla)\boldsymbol{v}] = -\nabla p + \eta\nabla^2\boldsymbol{v} \tag{2.3}$$

The reason why gravity and external forces are excluded is that in microfluidics, the dominating acting force within the microfluidic channel is viscosity. The left hand side of the equation can be interpreted as the inertial force densities and the right-hand side contains viscous and the applied force densities (pressure).

2.2 Viscosity

A factor that affects fluid flow is viscosity. Viscosity is the resistance or the internal friction of a fluids movement. Viscosity can be classified in two measures: dynamic viscosity and kinematic viscosity. The viscosity that is normally measured is dynamic viscosity.

Measuring the dynamic viscosity (symbol η) of a fluid is based on a theoretical model(Figure 2.1). This model contains a fluid that is placed in between two plates that are of area A. The bottom plate does not move; however, the top plate moves at a velocity v when pushed or pulled with a force F. The velocity of the moving plate illustrates the sheer stress of the fluid, and therefore shows the dynamic viscosity of the fluid.

The viscosity of the fluid is given by the force applied to the plate times the thickness of the fluid layer d divided by the velocity of the top plate, and the area of the plate 2.4. Dynamic viscosity has units of $Pa{\cdot}s$.

$$\mu = \frac{Fd}{vA} \quad [Pa{\cdot}s] \tag{2.4}$$

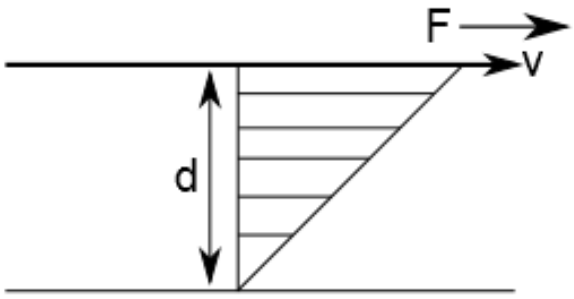

Figure 2.1: Theoretical model of viscosity

Another measure of viscosity is the kinematic viscosity [25, 34]. This is the ratio of the dynamic viscosity (η) and the density of a fluid (ρ), and is also known as the diffusion constant for momentum:

$$\nu \equiv \frac{\eta}{\rho} \tag{2.5}$$

2.3 Reynolds Numbers

Fluid flow can be broadly classified into two: turbulent and laminar. These type of flows can be illustrated by fluid streamlines. Laminar flows are usually drawn as lines that run along each other, remain col-linear and do not cross. Turbulent flows contain streamlines that do not run alongside each other and they may curl or swirl. The locations of these vortices at a given time may be random.

Modifying the Navier-Stokes equation for incompressible fluids (excluding body-forces) further by making it dimensionless, introduces a dimensionless number. This dimensionless number is the Reynolds Number (Re); a non-dimensional quantity that defines the gives the ratio of inertial to viscous forces:

$$Re = \frac{\rho v l}{\eta} \tag{2.6}$$

Where:

- Re is the Reynolds number

- $\boldsymbol{l}$ is the characteristic length

Reynolds numbers in excess of 10^3 show turbulent behaviours; a situation where inertial forces are much larger than viscous forces. Lower Reynolds numbers (typically $Re \ll 1$) show laminar flow, where no turbulence occurs inside a channel. This means that fluid flow is dominated by viscous drag rather than inertial forces.

2.4 Stokes Equation

Brody *et al* [3] studied fluid flow in microstructures and found that typical values for flowing water are $\mathbf{v} = 1 - 100\mu m/s$ and $\mathbf{l} = 10\mu m$. These values gives $Re = 10^{-3}$ to 10^{-5} which follows the definition of laminar flow. The low Reynolds numbers means that the left-hand side of the reduced Navier-Stokes equation (Equation 2.3) can be ignored because those terms represent inertial forces, which transforms the partial differential equation to a simple linear equation. Applying the assumption that fluid flow is determined entirely by the pressure distribution, the incompressibility constraint $\delta_i v_i = 0$, and the boundary conditions ($\mathbf{v} = 0$ at the walls), the equation becomes the Stokes equation:

$$\eta \nabla^2 = \nabla p \tag{2.7}$$

2.5 Surface Chemistry

Surface chemistry is a subtopic within physical chemistry, which outlines the physical chemistry of surfaces of multiple materials. It has a large influence on the motion of droplets in confined channels.

To describe the main concepts of surface chemistry which relate to the formation of droplets, the topic of surface energy will need to be understood. Surface energy of materials exists in multiple interfaces, however, for each interface, surface energy is interpreted differently. However, similar properties for each interface can be found in the general topic of surface energy. Such interfaces include: Liquid-Gas, Liquid-Liquid, Solid-Gas, Solid-Liquid, Solid-Liquid-Gas, and Solid-Liquid-Liquid interfaces.

The topic of surface energy leads into additional topics that describes how a surface can be hydrophobic, hydrophilic, lipophobic, or lipophobic. They provide a phenomenological explanation that helps us understand why fluid droplets remain as droplets or spread thinly over a surface. In the context of this thesis, they help us understand the behaviour of droplets travelling through microfluidic channels that are made from different materials that have these properties. A method used to quantify a materials hydrophobicity and/or lipophobicity, is to measure a water droplets or oil droplets contact angle.

2.5.1 Surface Energy

The observed contact angle is governed by surface energy. When changing the shape of a surface of any physical state, work is required. This is called surface energy. Surface energy is the amount of work per unit area needed to change the surface of a material. To conceptualise surface energy, a solid block made out of any material is considered. This solid material is made up of two groups of atoms within its lattice structure: surface atoms that contains open bonds that are not satisfied, and inner structural atoms that have sufficient bonds between neighbouring atoms.

When a new surface is created, one must break or create the intermolecular bonds between atoms. The amount of energy required to make or break these bonds is the surface energy of that material. The surface energy of liquids is classified differently as surface tension. The basic concept of surface tension is the same as surface energy, however, there are some differences when determining the surface tension of liquids. Surface tension is the work required to penetrate the outer layer of a liquid.

2.5.2 Liquid-Liquid Interfaces

In Liquid-Liquid systems such as water in oil droplets, surface tension and surface energy are referred to as interfacial tension and interfacial energy. When two pure liquids come into contact, there is an interfacial tension between the two liquids that can be observed. The critical solution temperature shows the critical temperature at which two liquids become completely miscible with each other. In quantifying of interfacial tension, the quantifying value relies on the distance from the critical solution temperature, or the miscibility of the liquids.

All droplet microfluidics rely on a high value of interfacial energy between the fluids in the continuous phase and the dispersed phase. An example in which high interfacial tension is required is the interaction between water and hydrocarbons. The value of interfacial energy between water and hydrocarbons is 50g/sec^2. Table 2.1 gives the interfacial tension between water and some organic liquids. It illustrates the immiscibility of organic liquids in water via interfacial tension. The column titled γ contains values of interfacial tension between water and specific organic liquids. The column titled Δ shows the differences in composition between the two phases.

Liquid	γ $(g{\cdot}sec^{-2})$	Δ **(per cent %)**
Hydrocarbons	About 50	About 100
Carbon tetrachloride	45	99.9
Nitrobenzene	26	99.5
Carbon disulphide	48	99.0
Ethyl ether	10.7	94
Aniline	5.85	91.5
Ethyl acetate	2.9	89
Isobutyl alcohol	2.1	75
Butyl alcohol	1.6	72

Table 2.1: Values of interfacial tension (γ) and chemical similarity (%) between water and organic liquids [1]

The basic rule that relates miscibility to interfacial tension is: when the miscibility is reduced, the interfacial tension increases, and when the miscibility is increased, the interfacial tension decreases.

Other factors that contribute to the quantity of interfacial tension include temperature and any external addition to the two-liquid system such as surfactants [1].

2.5.3 Lyophilic and Lyophobic Systems

The terms lyophobic (liquid-hating) and lyophilic (liquid-loving) are used to describe the tendency of a liquid to be attracted or repelled by a surface when in contact with the surface. If the liquid is aqueous (water), then the terms hydrophobic and hydrophilic are used. If the liquid is a lipid (oil-based), then the terms lipophobic and lipophilic are used. Clean surfaces that are normally lyophobic can be made lyophilic via an addition or reduction of material, and vice versa. For example, clean glass surfaces are normally hydrophilic, however, they can be made hydrophobic through the addition of a coating of wax; conversely, droplets in a hydrocarbon oil-in-water emulsion, which are normally hydrophobic, can be made hydrophilic by adding protein to the emulsion which the protein is adsorbed on to the droplet surfaces [29].

One of the main reasons that surfaces are either attracted (hydrophilic) or repelled (hydrophobic) by water is that water has the ability to form hydrogen bonds. Hydrogen bonds are intermolecular bonds that occurs when a small, highly charged electronegative atom with a lone pair of electrons shares its non-bonding atoms with a positively charged hydrogen atom, which is part of a polar molecule. If surface molecules cannot form hydrogen bonds with water, or have a tendency to repel via intermolecular forces, then the surface is hydrophobic.

When an oil is attracted or repelled by a surface, one talks about lipophilicity or lipophobicity. Lipids are naturally occurring organic compounds that are classified together on the basis of their common solubility properties. The main property that lipids are known for is that lipids are insoluble in water (due to water being a polar substance and no hydrogen bonds forming between lipid and water molecules), however, they are soluble in relatively non-polar, aprotic organic solvents. Aprotic solvents do not contain OH groups and cannot function as hydrogen-bond donors. Examples of aprotic solvents are hydrocarbons [2]. Consequently, for a surface to be relatively lipophilic, its molecular structure must be relatively non-polar.

2.6 Droplets on Surfaces

Droplet generation in most systems uses theory and mathematical models that are studied in droplet generation for solid-liquid-gas interfaces. It consists of the theory of a solid's wettability in solid-liquid interfaces, and the surface tension of a fluid droplet in liquid-gas interfaces. A quantitative measure of the surface tension of a droplet is obtained by measuring its contact angle.

2.6.1 Solid-Liquid Interfaces

The interfacial energy of solid-liquid interfaces is difficult to quantify because solids does not have a highly deformable surface hence they cannot dynamically change in response to the comparatively small surface energy interaction. Solid-liquid interfaces can be illustrated via the solid surfaces wettability and the measure of a liquid droplet's contact angle.

Wetting

Wetting is the displacement of a liquid on a surface by another fluid. This concept can only happen when the system contains three phases, in which two of them must be fluids. In this context, the surrounding air (which acts as the gas phase) is displaced by a liquid at the surface of a solid [11]. There are three types of wetting that can occur at solid-liquid interfaces:

- Spreading wetting: when a liquid already in contact with a solid spreads so that the solid-liquid and liquid-gas interfacial areas increases and the solid-gas interfacial areas decreases.
- Adhesional wetting: this involves a liquid that was not originally in contact with the solid substrate makes contact with it and adheres to it, decreasing the liquid-gas interfacial area.
- Immersional wetting: this involves the solid, which was not originally in contact with the liquid, is immersed completely with the liquid. The area of the liquid-gas interface does not change.

2.6.2 Surface Tension

Surface tension is a feature of the interface between liquid and gas, where the liquid seems to have been covered by a taut membrane. This membrane contains liquid molecules

that are attracted to each other via molecular attraction. Because of these molecular attractions, the liquid molecules tends to make its surface-to-volume ratio as small as possible. The geometrical shape that gives the smallest surface-to-volume ratio is a sphere, hence droplets without significant external forces are spherical in shape. This spherical shape provides the backbone to calculating the contact angle of a droplet.

In 1806, Pierre-Simon Laplace provided an illustration to explain a theory for surface tension [1] (Figure 2.2). Consider a line **OO** that represents the boundary between liquid and gas. Movement of a small group of molecules occurs within a sphere, and a circle is drawn as a cross-section of this sphere. Consider a molecule positioned in the centre of the circle ***a***. Molecules within this sphere produce a noticeable attraction toward the central molecule, while forces that are observed outside this sphere are neglected. Since molecule ***a*** is far from the surface, the whole sphere is within the liquid and no external force acts on the molecule.

Consider another molecule inside ***b***, where part of the sphere is outside of the liquid. The part of the molecule that is inside the liquid, is attracted towards the interior of the liquid and is not counterbalanced by any additional forces. To increase the surface area of the liquid, this requires adding the number of molecules that are situated in the surface layer, which requires work against the intermolecular forces. This particular theory raises a question on the size of the sphere which represents molecular action. If the laws of molecular attraction were known, then the radius of the sphere would be known.

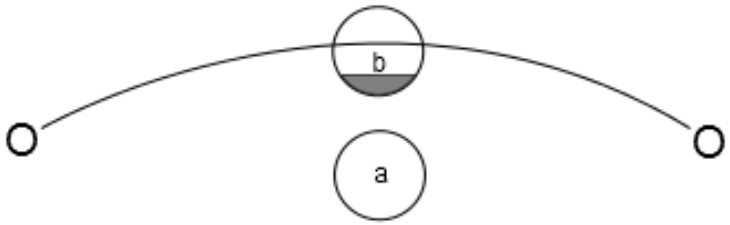

Figure 2.2: Laplace's explanation of surface tension

2.6.3 Contact Angles

Contact angles are found in gas-liquid-solid systems where a droplet is formed on a surface when an equilibrium between three interfacial energies (γ) is reached (Figure 2.3). These energies are:

- γ_{LG} - Liquid-gas interfacial energy
- γ_{SL} - Solid-liquid interfacial energy

- γ_{SG} - Solid-gas interfacial energy

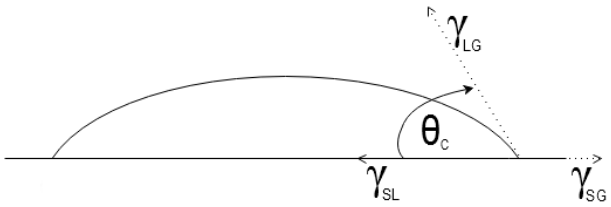

Figure 2.3: A droplet on a surface, showing the three interfacial energies involved to form the droplet's contact angle

Equation 2.8 illustrates the horizontal forces in equilibrium for each interfacial energy. An issue with this equation is that the interfacial energies of the solid-liquid and solid-gas interfaces is very hard to quantify.

$$\gamma_{SG} = \gamma_{SL} + \gamma_{LG} \cos\theta \tag{2.8}$$

Another function that is used to illustrate the adhesion of the droplet to the solid surface, is the work of adhesion (Equation 2.9) [1]:

$$W_a = \gamma_{LG} + \gamma_{SG} - \gamma_{SL} \tag{2.9}$$

Combining equations 2.8 and 2.9 produces a formula that contains measurable quantities:

$$W_a = \gamma_{LG}(1 + \cos\theta) \tag{2.10}$$

θ is the contact angle that can be measured via experimentation. A large contact angle ($\theta \rightarrow 180°$) indicates that the molecules within this droplet are repelling the surface, and a smaller contact angle ($\theta \rightarrow 0°$) indicates that the molecules are attracted to the surface. The reason for the attraction and repulsion to the surface is mainly due to the intermolecular forces between the molecules in the droplet and the molecules within the surface. In the case of water and lipids, the main intermolecular forces that contribute to the size of the contact are hydrogen bonds. The attraction and repulsion of water molecules inside a water droplet can illustrate how hydrophilic or hydrophobic a surface is.

Chapter 3

Background

Microfluidic devices have been developed by many people as a way to downscale a traditional fluidic system (which the fluidic channels are usually measured in scales greater than millimeter dimensions). These scaled systems have allowed a reduction in fluid consummables and reagents, reduced process times, and enable new phenomena.

This chapter briefly summarises a handful of recent relevant guides and work that informs this thesis. The topics that this literature review will look at are microfluidic technology and droplet generation, and drug delivery, needles and implants.

3.1 Microfluidic Technology and Droplet Generation

Microfluidics has been a growing field for research due to the potential that it can provide within a variety of fields including medicine, biotechnology, and chemistry. Applications include drug delivery, point-of-care diagnostic chips, organic synthesis, and micro-reactors. Droplet-based microfluidics, the focus of this project, is a branch topic of microfluidics that creates and uses discrete volumes of droplets within an immiscible fluid (a droplet carrier).

Technology based on microfluidics and droplet microfluidics has great potential in chemical analysis and synthesis in typical laboratory operations, because they enable the use of a fraction of the volume of reagents in significantly shorter times. Volumes of reagents can be reduced from millilitres to microlitres and nanolitres, and reaction times of chemical processes can be reduced from hours and minutes to seconds, due to convective mixing and the diffusion of fluids within a small volume [31].

Different methods used to create droplets within microfluidic channels generally involve geometry configurations such as T-junction (Figure 3.2) or flow-focusing (Figure 3.1) configurations, or electrically control droplets by integrating electrodes into microfluidic

devices, for example, a device that produces surface acoustic waves to control the volume of water droplets.

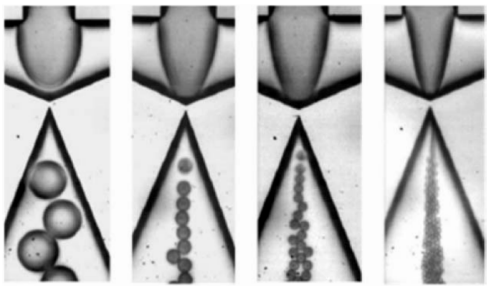

Figure 3.1: Formation of droplets using flow focusing design [31]

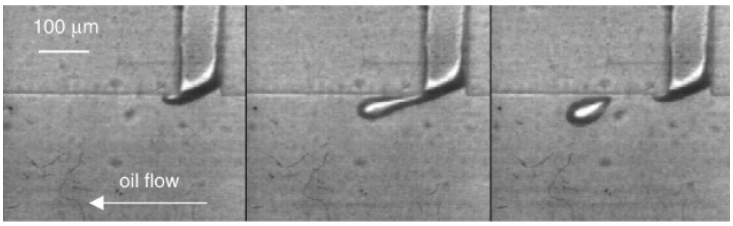

Figure 3.2: Formation of droplets using T-Junction configuration [17]

Foley *et al* developed a microfluidic device that utilises convection enhanced delivery (CED) for neural drug delivery [10]. CED involves infusing drugs locally into tissue through a needle into the brain (such as the prefrontal cortex), where the delivery is dependent on convection, which enhances drug penetration into tissue compared to diffusion delivery. Fabrication of these devices involves utilising standard MEMS fabrication techniques to make the microfluidic channel, and hot embossing poly (DL-lactide-*co*-glycolide) (PLGA, a biodegradable polyester) to fabricate the biodegradable insertion scaffolds. This device delivers the drug directly, which brings a question of the device's chemical resolution, as stated in the research question: does the device deliver an accurate amount of drug within nanolitre to picolitre resolution?

Applications of microfluidic devices in neural drug delivery involves specific challenges that needs to be addressed. Rathnasingham *et al* developed a systematic method [26] to calibrate, test, and optimise fluid delivery devices that addresses the flow issues such as the manipulation of very low volumes (nanolitres), discrete pulse delivery (which is an important topic for droplet-on-demand devices), and fluid diffusion in the neural environment. Although this paper does not involve fabrication of a specific device, it provides an overview of the characteristics that a microfluidic device should have, in order to use this method to calibrate and analyse the device's ability in discrete pulse delivery.

3.1.1 Generating Droplets on Demand

To generate droplets in microfluidic channels, researchers in the field of microfluidics have developed different droplet generation techniques where the generation relies on either the physical geometry of the microfluidic channel, or integrating electrodes into the device. Generating droplets on demand is useful because it allows control over the size of the droplet in the continuous phase, and the time when it needs to be delivered.

Galas *et al* [12] fabricated a device that combines the T-junction configuration and a switching component to connect a microfluidic device to external fluid devices. The device aims to accurately control individual droplets size and drop production rate dynamically. The droplet distribution device is called an active connector (AC), and is fabricated in a small PDMS cube that contains two perpendicular PDMS channels bound on top of each other, with a thin layer of PDMS separating them. The bottom channel contains the fluid in which droplets will be generated with, and the top channel (filled with water) controls the switching aspect of the AC. When pressure is applied to the top channel by a computer-controlled air pressure source, the thin membrane stretches and blocks the bottom channel, effectively closing it.

By using computer-controlled pressure flow, droplet generation can be easily controlled conceptually by a switch. Droplet generation is done by a T-junction with the continuous phase filled with a mixture of mineral oils: span 80 (4.5% (volume/volume)), tween 80 (0.4% (volume/volume)), and triton X100 (0.05% (volume/volume)).

Collins *et al* [7] developed a method to produce picolitre scale droplets for a water-in-oil microfluidic system via surface acoustic waves (SAW). The SAW microfluidic devices controls the volume of these droplets, which are defined by the applied power, duration of the force and the microfluidic channels geometry. The device itself is comprised of a microfluidic chamber, which is placed on top of a SAW device.

The microfluidic channel was made using photolithography methods by coating a lithium niobate substrate with 70 nm of SiO_2, which is then embossed with a PDMS mould, which will contain the features of the microfluidic channel. The microfluidic channel contains a continuous oil phase and a dispersed water phase that is similar in structure to a T-junction configuration, with the SAW device situated underneath the water phase to control the volume of the water droplet.

3.1.2 Controlling Droplet Size

Dangla *et al* [8] discovered a way to generate different sized droplets by only changing a single parameter in the fabrication of the microfluidic channel. Microfluidic droplets

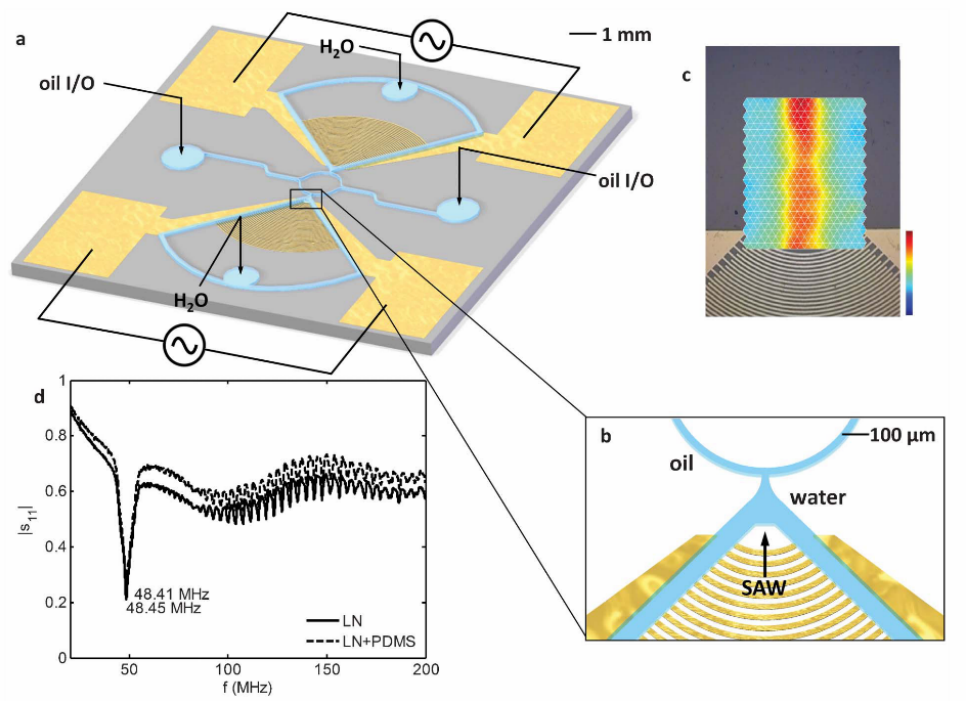

Figure 3.3: SAW-controlled droplet generation system. (c) illustrates the RMS amplitude distribution of the electrode pads producing SAW. [7]

are typically created at a junction where the continuous and disperse phases meet. The disperse phase fluid starts to form a droplet at the junction where it finally breaks off into the continuous phase due to hydrodynamic forces. These forces involve many parameters such as the flow rates, geometric parameters, and fluid properties (for example viscosity). This poses a problem of changing one parameter, which in turn will affect the others. This paper explores if changing the gradients of confinement alone is sufficient enough to generate droplets.

The main experiment was to change the angle of the disperse phase channel where the droplet forms into a reservoir (without needing to use hydrodynamic forces to break off the droplet) (Figure 3.4. This experiment assumes that the pressure used to drive the continuous and dispersed phase, and the fluids used for the two phases are constant. One of the tests performed was when the inclination angle is at zero degrees or the plane of the disperse phase is parallel to the plane of the substrate itself. The droplet formed from this will grow indefinitely and will not break into the reservoir.

Nisisako *et al* [17], researched droplet formation within a T-junction microfluidic channel (Figure 3.2). The microfluidic channel was fabricated on a PMMA substrate using a $100\mu m$ diameter end mill. The continuous oil phase channels width is $500\mu m$, and the dispersed water phase channels width is $100\mu m$. Both channels depth is made to be $100\mu m$, and the channel is lidded with adhesive tape.

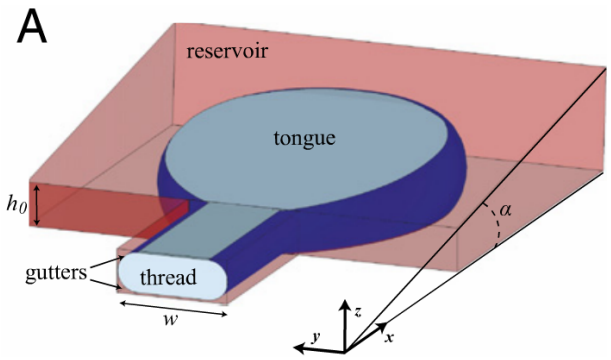

Figure 3.4: Formation of a droplet into a reserviour. The angle (α) is changed to change the size of the droplet without relying on hydrodynamic forces [8]

The tests that were performed includes measuring the driving pressure needed for both continuous and disperse phases to produce water droplets that are $100\mu m$ in diameter. The oil used in the continuous phase is high oleic sunflower oil (triolen, 80%), and the water used is ultra-pure water.

3.2 Drug Delivery, Needles and Implants

There have been a rise in the development of novel devices that can be used for medical applications. Related applications to microfluidic needles include drug delivery and implants.

A magnetically controlled Micro-electromechanical Systems (MEMS) device was created by Pirmoradi *et al* [24]. This device was specifically designed for drug delivery, addressing the issue of conventional drug delivery limitations by having the ability to allow precise control over drug release which is typically suitable for implants. It can be used in the treatment of glaucoma (chronic ocular disease), control of chronic pain or various localised tumours.

Fabrication of the device involves methods of photolithography, spin-coating, and oxygen-plasma treatment, to create a mechanism that is akin to squeezing water out of a flexible bottle. Precise control of drug release involves remotely actuating the device by a magnetic field, pulling an elastic magnetic membrane, which increases the pressure inside a drug reservoir to push the drug out. This device allows for on-demand drug release.

Neural stimulation has been used in many types of neural disorder treatments, typically via electrical stimulation. A different kind of stimulation that uses light of a defined wavelength to directly stimulate neurons that are already genetically modified to release light-sensitive proteins when excited by light. This method is called optogenetics. Rubehn *et al* [21, 27] developed a polymer-based neural microimplant that uses optogenetics 3.5. The implant itself combines three essential optogenetics processes that are used to stimulate specific neurons within a brain into one device:

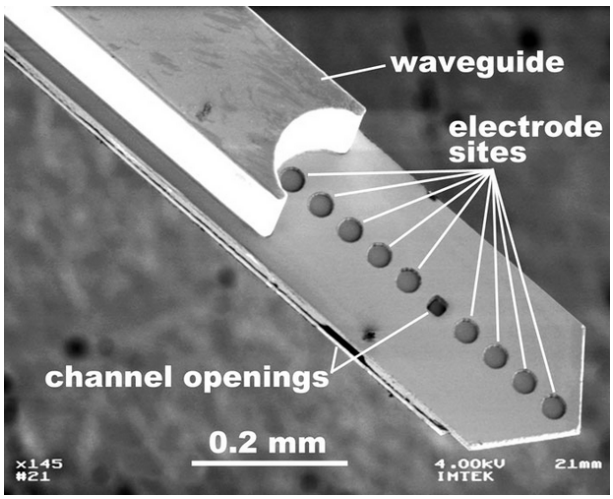

Figure 3.5: Microfluidic needle used for optogenetics [21, 27]

- Delivery of gene-carrying fluids using a microfluidic channel
- Stimulation of neurons with light via an optical waveguide
- Recording the brain cells electrical response using microelectrodes

Akin to brain control, it can lead to breakthroughs towards curing Parkinsons disease, addiction, depression, and spinal-cord injuries. Manufacturing of the needle involves process technology, used to manufacture MEMS devices. The needle is made out of polymers; in competition with silicon-based approaches in other implants.

An application that uses microfluidic technology in implants is the eye sensor for glaucoma patients. This study shows the great potential of microfluidic technology used in biomedical science applications. Glaucoma is the second-common cause of blindness in the world. It occurs by the increase of eyeball fluid pressure, which can build up enough to damage the optic nerve [23].

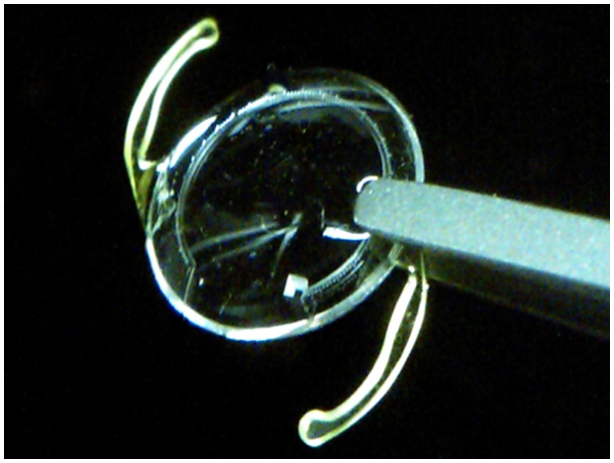

Figure 3.6: The sensor conatins a microfluidic channel which actively monitors eye pressure in glaucoma patients [23]

The microchannel has the width and depth of 50 μm which is run around the edges of a lens. One end connects to a tiny gas reservoir, while the other connects to the aqueous eyeball fluid. The sensor will be surgically implanted into a patient's eye. Once implanted, pressure drives the eyeball fluid into the microchannel, compressing the gas until the pressures of the gas and fluid reaches equilibrium. A doctor can detect increased eyeball fluid pressure by using a smartphone camera, equipped with an optical adatper and imaging analysis aoftware to detect the position of the liquid.

Chapter 4

Microfluidic Device Design

4.1 Microfluidic Channel Design

Microfluidic droplets can be formed via various techniques such as changing the geometry of the channel in T-junction and flow-focusing configurations, and integrating electrodes into microfluidic devices to control droplet formation via electrical pulses [31]. One of the project outcomes is that the needle will have the capability to administer multiple drugs in the one needle. The needle must also be simple to manufacture, hence the T-junction configuration design is chosen for droplet configuration.

After choosing the method of droplet generation, one has to consider other parameters that will affect the generation of a water droplet in the water-in-oil system. These parameters include the length of channels upstream and downstream of the T-junction and the disperse phase (water phase), the pressure used to drive each channel, and the viscosities of both oil and water. The channel length was considered in the design to minimise the operating pressure differential required. A primary design question is to find the length of both channels so the oil and water reaches the T-Junction with similar pressures. This will facilitate droplet formation. Due to resources restraints during the development of the project, the only oil available was Fomblin 25/6 vacuum pump oil. The oil also acts as a proof-of-concept idea which demonstrates that a variety of different oils can be used for a water-in-oil droplet-on-demand microfluidic system.

4.1.1 Electrical Circuit Analysis for Microfluidic Channel Design

Tondeur *et al* [32] developed an analytical approach which claims that fluidic channel analysis can be performed in the same manner as electrical circuit "ladder" analysis.

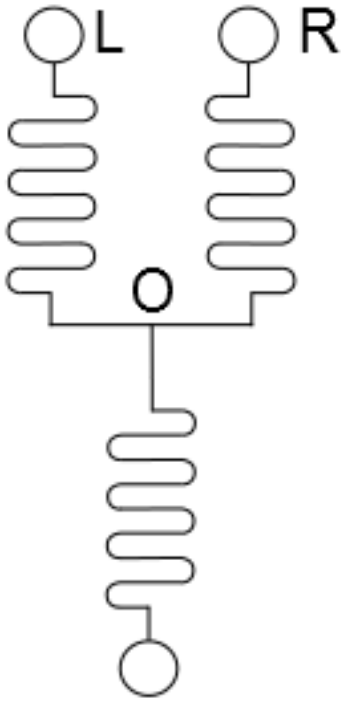

Figure 4.1: Illustration of the T-junction channel, similar to an electronic circuit

This analogy was used when designing the microfluidic channel and includes the following assumptions:

- External body forces, such as gravity and electrical forces are neglected
- Fluid flows at low Reynolds numbers, or in laminar flow

Based on this analogy:

- The pressure (p) used to drive each fluid is analogous to the electrical voltage (V)
- The width and depth of the channel (l) and the viscosity of the fluid (μ) that runs through that channel are used to calculate an equivalent electrical resistance (R). As every part of the device will have the same width and depth, these parameters can be ignored and an equivalent resistance is given by$R = \mu \times l$.
- The volume flux of the fluid travelling through the microfluidic channel is analogous to the electrical current (I).

Figure 4.1 illustrates the basic T-junction channel containing two input channels labelled **L** (left-for oil) and **R** (right-for water), with the intersection where the two channels meet is labelled **O**. Since parts of the microfluidic channel are defined as an electronic

circuit, the problem changes to finding the length of each channel so that there is more oil (continuous phase) than water (i.e. $I_{oil} > I_{water}$) are in equilibrium, i.e. $I_{left} = I_{right}$. Using Ohms Law ($V = IR \Rightarrow I = \frac{V}{R}$), the ratio of the channels' length can be found:

$$\frac{V_{left}}{R_{left}} = \frac{V_{right}}{R_{right}} \tag{4.1}$$

$$\frac{V_{left}}{\mu_{left} \times L_{left}} = \frac{V_{right}}{\mu_{right} \times L_{right}} \tag{4.2}$$

$$\frac{V_{left} \times \mu_{right}}{V_{right} \times \mu_{left}} = \frac{L_{left}}{L_{right}} \tag{4.3}$$

Assuming that the viscosity of water is 1.00×10^{-3} $Pa{\cdot}s$, the viscosity of oil is 5.22 $Pa{\cdot}s$ (by finding from the Edwards Limited website [9] that the volume of the Fomblin 25/6 oil is 529 mL for 1 kg mass, the kinematic viscosity is 276 cSt, and then using Equation 2.5 to find the dynamic viscosity), and the same, constant pressure is applied to both channels, we find that the length of the water channel must be approximately 5000 times greater than the oil channel. In this design, we were limited to uniform width channels where the oil channel is just three times longer than the water channel. Ultimately, the oil channel length was 35.27 mm and the water channel length was 105.01 mm. Future designs may use a wider oil channel, a longer water channel and an oil with a lower viscosity. After a conceptual drawing, the microfluidic channel was drawn as a 3D model in AutoCAD. (9mm port config.)

4.1.2 CAD Design

The designed channel was drawn in CAD to illustrate a 3D model of the microfluidic channel inside a thermoplastic substrate.The design was sent to the Australian National Fabrication Facility at the University of South Australia (ANFF-SA) to micro machine the microfluidic design onto a PMMA substrate. The substrate has the same dimensions as a standard laboratory glass slide (75 $mm \times 25$ mm). This size will make the embossing process much easier to perform using standardised dimensions. This machined PMMA device can be used as is or used in a soft embossing process to create replicates (see Chapter 5) for use in the embossing process. According to ANNF, machining the designed channel into COC is not preferred due to the resulting surface appearance after machining will not be clear, hence making it difficult to view the droplet generation inside the microfluidic channel.

Figure 4.2 illustrates the master PMMA slide containing the designed microfluidic channel, and Figure 4.3 shows the substrate with a lid bonded on top of the slide. The ports were made in a configuration, which will become a standardised design throughout future channel designs in a 9 $mm \times 9$ mm square. This port spacing is based on the spacing of a 96 sample well microtiter plate and is a standard port configuration for devices used in our lab. The lid will contain holes for the ports and a tapered hole, specifically for the output at the tip of the needle where the membrane will be bonded.

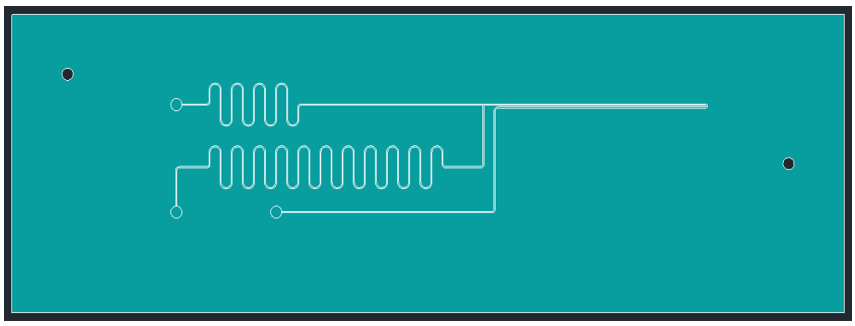

Figure 4.2: Top view of the microfluidic channel

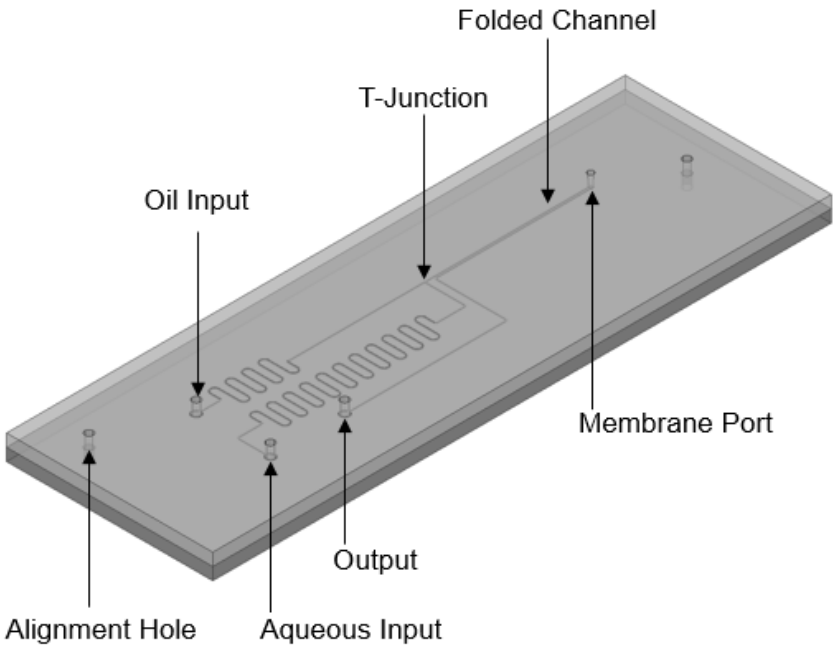

Figure 4.3: Isometric view of the microfluidic channel, with a COC lid

In addition to the port holes, two additional holes were drawn as alignment holes to ensure that the port holes and the membrane port hole in the lid aligns with the input and output ports for continuous and disperse phases, and the tip of the needle, respectively during bonding the substrate and lid. The centre of the top-left alignment hole is placed

5 *mm* from the top and left of the edge. The second alignment hole is placed 12.5 *mm* from the top edge and 5 *mm* from the right edge. To indicate that the dispersed water phase is three times as long as the continuous oil phase, the resistor part of the channel is extended to three times the oil phases resistor length. The substrate will then eventually be machined cut into a needle shape, which is why the length of the channel after the T-junction is extended.

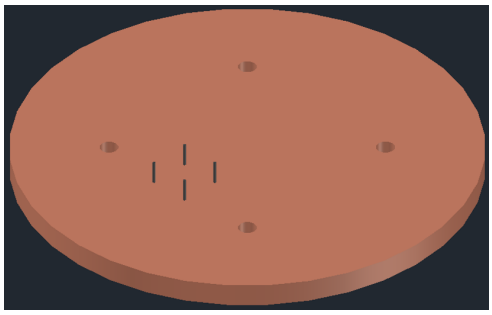

Figure 4.4: Top isometric view of the chuck used for the confocal microscope

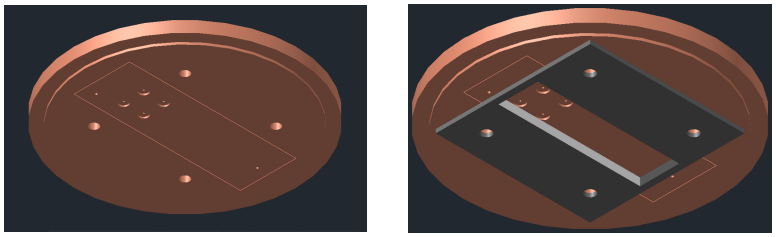

(a) Without steel plate **(b)** With the steel plate

Figure 4.5: Bottom isometric view of the chuck, where the microfluidic chip is held

To hold the sample for the confocal microscope, a chuck was developed using CAD, which contains four needle ports (Figure 4.4) to attach tubing (0.2 *mm* outer diameter, 0.1 *mm* inner diameter) to. The material used to fabricate it is Perspex, to allow the inverted epifluorescent microscope to image the microfluidic channel. The microfluidic chip is placed underneath the chuck, where the port holes are aligned to the needle ports on the chuck.

At the bottom of each needle port (Figure 4.5a), contains a concentric port which has a larger diameter than the needle port to hold an o-ring. This prevents fluid from leaking at the ports when inserting the fluid into the microfluidic chip. A hollowed-out steel plate (Figure 4.5b) attaches to the bottom part of the chuck, which tightly holds the sample to the chuck.

4.2 Thermoplastic Material Selection

Microfluidic channels have been fabricated in various thermoplastic substrates. Carvalho *et al* [5] fabricated a microfluidic channel in PMMA, Chen's [6] chemistrode is made out of PDMS with Teflon tubing inserted. For the final water-in-oil microfluidic system to run in approximately ideal conditions, the water channel must be hydrophobic as possible to prevent water residue to adhere to parts of the channel, leading to an increased chance of coalescence between the water droplets and the continuous oil phase. Measuring the contact angle of a water droplet on a surface can determine hydrophobicity and give an indication of which material is best for the fabrication of the microfluidic droplet device because this will ultimately be implanted. Brittle materials like glass are not suitable.

4.2.1 Method

Six different materials were tested during this experiment by applying water droplets on each surface using a pipette and placing each of them on its side, under a digtial camera-fitted microscope. The six surfaces tested were:

- Cyclic Olefin Copolymer (COC)
- Standard Laboratory Glass Slide
- Overhead Transparency (cellulose acetate)
- Polystyrene
- Poly Methyl Methacrylate (PMMA)
- Polycarbonate

Each surface was cleaned by washing with laboratory detergent and water in an ultrasonic bath. Multiple photos of water droplets were taken and the angle of each droplet were measured (Figure 4.6). The average and standard deviation for each contact angle were calculated and collated into a graph (Figure 4.7).

4.2.2 Results

To have a reference of a known contact angle, a glass slide was chosen as the control, because it is known that its surface is hydrophilic. Water droplets placed on polystyrene and PMMA contained the lowest contact angle which is comparable or less than the contact angle resulting from a glass slide, hence their surfaces are deemed hydrophilic.

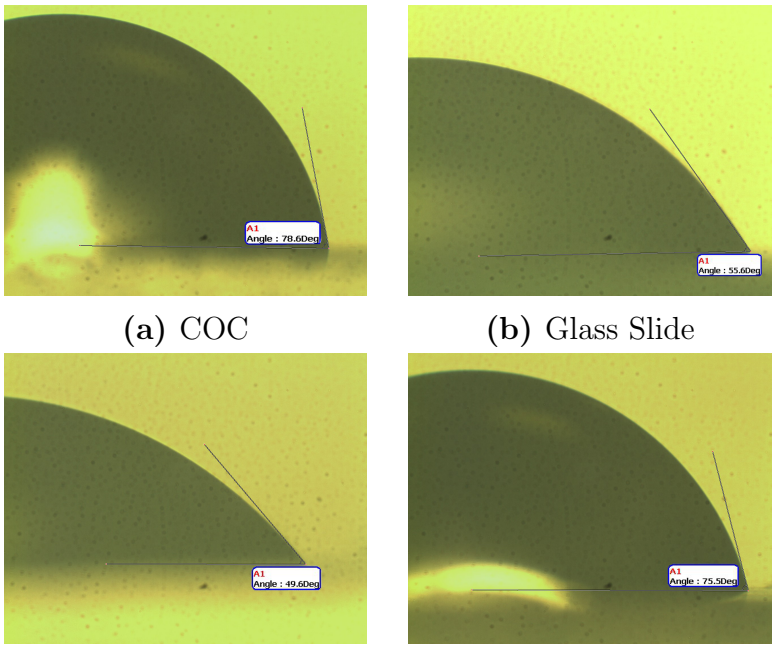

(a) COC **(b)** Glass Slide

(c) PMMA **(d)** Polycarbonate

Figure 4.6: Image captures of droplets on different surfaces

The surfaces that produced higher contact angles were COC, overhead transparency and polycarbonate, hence they are deemed hydrophobic.

4.2.3 Discussion

The standard deviation of the overhead transparency and polystyrene was relatively high, meaning that the results measured fell into a varied range of angles. This could be due to the droplets being affected by gravity, while measurements were recorded. To confirm the results, a greater range of thermoplastics should be tested.

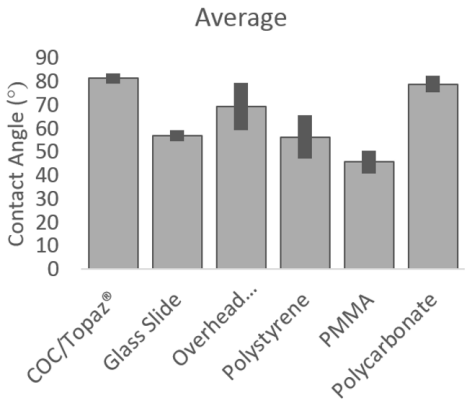

Figure 4.7: Comparison of each material's contact angle

4.2.4 Conclusion

The experimental outcome was to determine the material that is the most hydrophobic, so that it can be used for the fabrication of the microfluidic implant. From the averaged results, COC is shown to be the most hydrophobic and is therefore the material that will be used to fabricate the prototype implant. The material is also suitable for low-cost volume manufacturing.

Chapter 5

Fabrication

5.1 Development of the Embossing Method

Fabrication of microfluidic channels are usually very expensive, usually involving photolithography to create a mould, and using machinery for applying pressure and heat to stamp the mould into a blank plastic. Narasimhan and Papautsky [16] developed a method to create a poly dimethyl siloxane (PDMS) mould by creating planar casting templates, using photolithography techniques. Lomas *et al* [15] built their own embossing machine and fabricated an aluminium mould using a high precision CNC milling machine with 1 μm resolution. Both of these methods require machines, which can be expensive to purchase for mass-scale production, hence an easier, cheaper method has been developed. According to the ANFF in University of South Australia, machining a 100 micrometre microfluidic channel into COC is not preferred because the resulting product will have a poor surface finish and is likely to hinder droplet flow, hence machining in their preferred material was done.

5.1.1 Experimental Outcome

The outcome of this experiment is to develop and find the optimal embossing method for embossing a PMMA mould into a cyclic olefin copolymer (COC) substrate, through the use of an elastomeric intermediate. Goral *et al* [13] developed a simple method for embossing a PDMS mould - fabricated using soft lithography - into polystyrene, using $\frac{3}{4}$ inch binder clips and a laboratory oven. This experiment will use that same method however, there are some parameters that will be changed for embossing into COC.

5.1.2 Method

Soft Lithography of PDMS Mould from machined PMMA Device

The PDMS mould was created using a mixture of Sylgard 184 Silicone elastomer base and Sylgrard 184 Silicone elastomer curing agent in a 10:1 volume/volume ratio. After a couple of minutes of mixing, it was placed into a desiccator, where it was placed under vacuum (of around $-90\ kPa$) for 15 minutes, to release any air bubbles that may be trapped within the mixture.

A standard laboratory glass slide ($75\ mm \times 25\ mm$) or a large laboratory glass slide ($75\ mm \times 50\ mm$) was placed into a plasma cleaner/etcher (March©) to ensure that the hardened PDMS gel will stick to the glass slide. It was left in the plasma cleaner for two minutes. The mixture is poured onto the glass slide where it is evenly distributed throughout the slide to ensure a flat surface when making a print of the channel.

The PMMA master slide is placed on top of the PDMS, with the actual channel facing downwards. The whole assembly is placed into a standard laboratory oven overnight at 75°C. Using gravity and capillary forces as the downward force, the PDMS mixture is allowed to fill up all the crevices within the PMMA master slide.

Once the PDMS mixture is hardened, it is separated from the PMMA master slide before the assembly cools to room temperature. Figure 5.1 shows the completed PDMS mould on a standard laboratory glass slide, based on the designed microfluidic channel in AutoCAD.

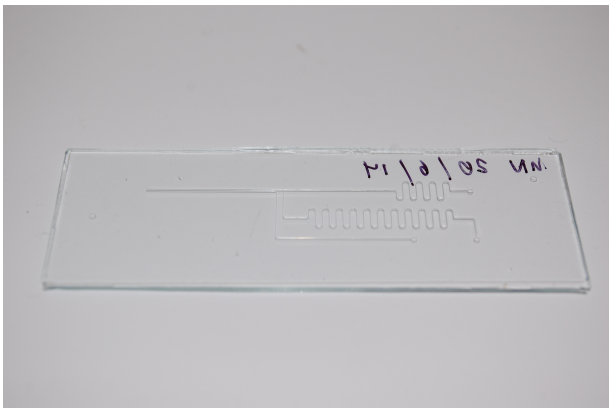

Figure 5.1: Glass and PDMS mould created for the embossing method. The PDMS layer is approximately 250 μm thick

Hot Embossing Method

The hot embossing method is based on the method given by Goral *et al.* Since the length of the PDMS mould is longer, more clips will be used. For an optimal emboss, all glass

slides, the PDMS mould, and the COC slide should be cleaned from any dust particles. Cleaning each slide involves placing each slide into a small container with detergent and water in a 10:1 volume/volume ratio, and placing them in an ultrasound bath. Each slide is exposed to ultrasound for five minutes.

The COC Topaz slides were bought from microfluidic ChipShop, however, they did not provide information on the chemical and mechanical properties for the grade of COC used, hence, the property of the COC's heat deflection temperature was experimentally observed.

The COC and glass/PDMS slides are assembled by placing the COC slide on top of the PDMS mould, with a glass slide on top, and on the bottom. The additional glass slides distribute the clamping force of the binder clips. The whole assembly is held together via a number of binder clips in a certain orientation. Each method in the results section (Section 5.1.3) describes a different orientation of each binder clip. The binder clip orientation was determined to apply as much force to as much of the surface area of the assembly itself as possible. The whole assembly is placed into either a standard laboratory oven or a vacuum laboratory oven for a certain amount of time. After the specified time has elapsed, the assembly is taken out, and is let to cool to room temperature before disassembling.

Measurements of the channels at certain points are taken by a profiler. Other features of the embossed microfluidic channel can be analysed using a microscope, especially when checking that the channels are embossed properly.

Binder Clip Force Calculation

In addition to developing the embossing process, an experiment was done to calculate the amount of force that each binder clip applies at different opening distances. Goral *et al.* made similar force measurements for their binder clips, using an Instron®Instrument. The force of the binder clips were measured using a spring scale at various opening distances.

Figure 5.2 shows the measured and forecasted force of two different sized binder clips. Similar to Gorals results for $\frac{3}{4}$ inch binder clips, the force measured shows that the pressure applied to the embossing method is time dependent due to the COC substrate changing its thickness under high temperature. Initially, the thickness of the whole assembly is approximately 4 mm, since each slide has a thickness of 1 mm.

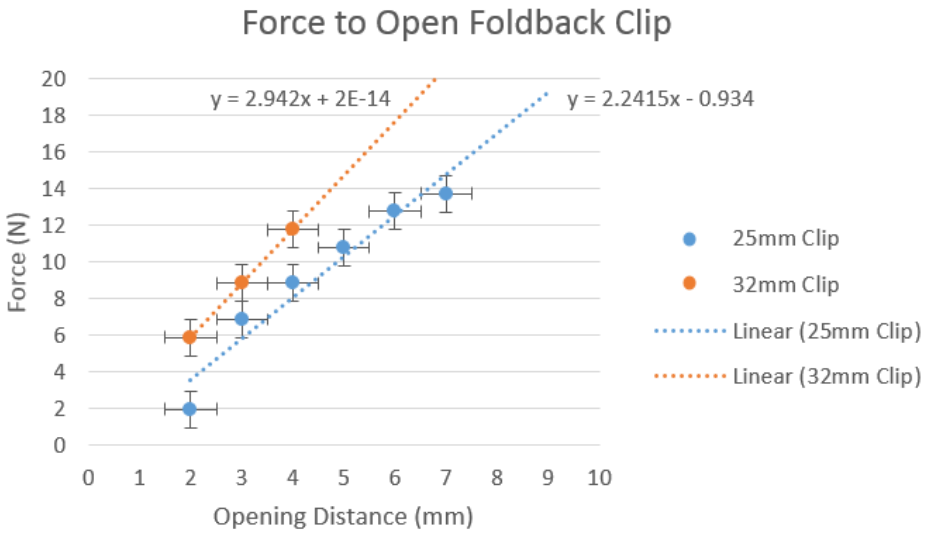

Figure 5.2: Line graph, showing the force measured at different opening distances (in N/mm)

5.1.3 Results of Embossing Methods

Each method iteration were slightly different in terms of what temperature was used and how long the force and heat were applied. The first six methods were a test to see the capabilities of embossing using a larger glass slide. The following methods used a PDMS mould, fabricated on top of a standard laboratory glass slide. Table 5.1 summarises the embossing temperature and time used for each experimental iteration.

Height measurements of the channel, for each method were taken at six specific points:

- Each of the three input/output ports' entry/exit channel
- The T-Junction where the oil channel and the water channel meet
- Two parallel channels, on the way to the tip of the needle
- Tip of the needle

Method 1

Two 32 *mm* binder clips are placed on both sides of the large glass slide assembly as shown in Figure 5.3a. The force generated from the two clips was approximately 11.5 *N*. The whole assembly is placed into a standard laboratory oven (Thermoline Scientific©) at 165°C for 15 minutes.

The height of the channel was measured at the tip of the needle (Figure 5.4). This is to see the cross-section of the channel to ensure that the channel is embossed evenly.

Method No.	Temperature (°C)	Time	Pressure (N)
1	165	15 mins	23
2	165	15 mins	23
3	175	15 mins	23
4	155	15 mins	41
5	140	10 mins	41
6	165	15 mins	41
7	180	15 mins	54
8	180	25 mins	54
9	165-170	25 mins	54
-	155	20 mins	54
10	166	25 mins	54
11	170	$>$ 1 hr	54
12	165-170	1.5-2 hrs	54
13	150-155	1.5-2 hrs	54
14	170	2 hrs 40 mins	54
15	155-160	15 mins	54

Table 5.1: Various iterations of the embossing method

We have found that this feature is the most difficult to reproduce in the embossed parts. Figure 5.5 illustrates the graph created by the profiler. The graph shows that the channels were not embossed properly because the middle section of the cross-section is expected to be the same height as the height of the plastic slide. Air bubbles formed throughout the slide, which suggests that air is being trapped in between the COC slide and the PDMS mould while the embossing assembly was being put together. These may be caused by gases expanding while being heated.

Figure 5.6 shows the resulting embossed device at the T-junction, the leading channels, and the tip of the needle. The darker areas shows parts of the channel that were embossed, and the lighter areas are parts of the COC slide that are untouched by the PDMS mould. The height of the channel at this point is 94.7 μm, which comparatively close to the required height, which is 100 μm. The appearance of the channels are not well defined, which means that the channels are not embossed well. The height of the T-junction was measured to be approximately 50 μm.

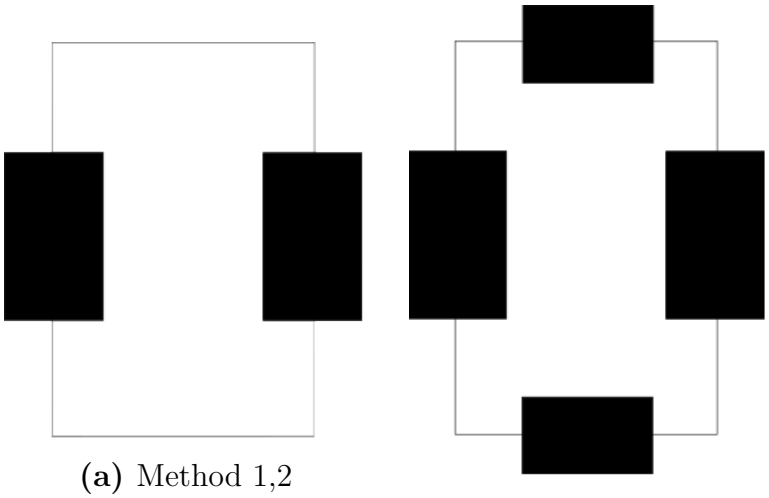

(a) Method 1,2

(b) Method 3

Figure 5.3: Configuration of the binder clips for specific methods

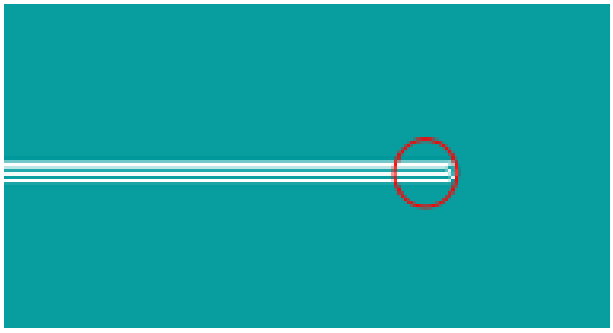

Figure 5.4: The tip of the needle, where the main height channel measurements were made

Method 2

The embossing assembly was done similarly to Method 1, however, the whole assembly is placed into a desiccator for 15 minutes to remove any air bubbles that may be trapped within the assembly. When the needle tip is measured, the middle part of the cross-section is at the same height as the left and right parts, however, when the channel was measured at the middle of the needle, the previous graph from Figure 5.5 appears again.

Method 3

Figure 5.3b illustrates the binder clip configuration that was used in this iteration. This is similar to the two previous methods, however, two 25 mm clips were added to the two empty ends to apply more force to the embossing tool. The force generated from the four clips was approximately 41 N The resulting graph from the profiler is similar to the previous graph that appeared in Methods 1 and 2.

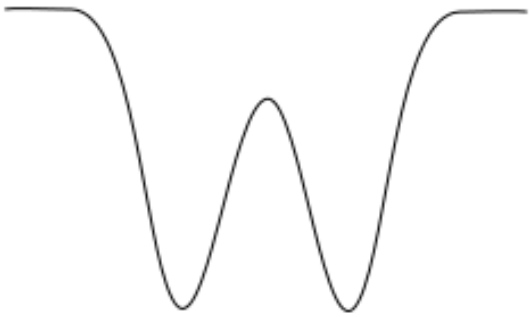

Figure 5.5: Illustration of the profiler graph showing the imperfect emboss in Method 1

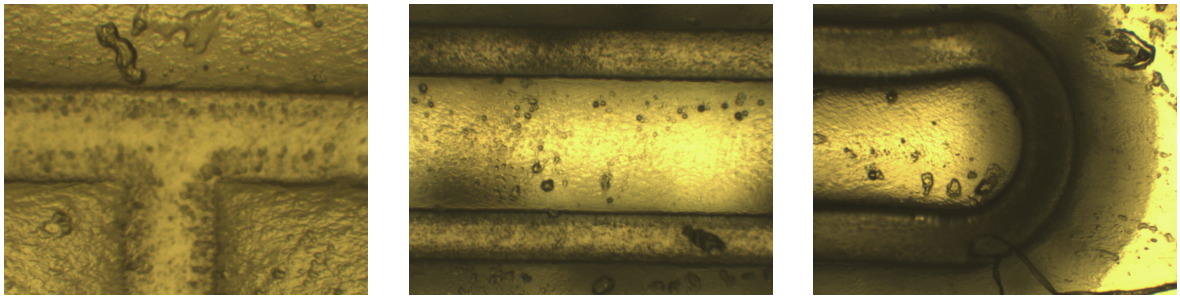

(a) T Junction **(b)** Channels **(c)** Tip

Figure 5.6: Resulting images of the device using Method 1

Method 4 and 5

Both of these methods involve preheating the COC substrate at 70°C and 140°C (for each respective method) in a laboratory oven for 10 minutes. The emboss tool is assembled and is placed into the desiccator until the laboratory oven preheats to 155°C. The assembly is then placed into the oven for 15 minutes and let cool to room temperature, before disassembling.

Both results produced cleaner substrates, with less bubbles forming, however, the profiler measured the channels cross-sections to still have the middle section to be lower than the left and right sections of the cross-section similar to Method 1.

Method 6

To reduce the amount of air bubbles that may be trapped between the PDMS mould and the COC substrate, a vacuum oven was used. The vacuum oven was preheated to above the glass transition temperature of COC (by trial and error, was found to be approximately 155°C), while the COC substrate was preheated in a different oven at 145°C for 15 minutes. The embossing assembly was placed into the vacuum oven for 15 minutes. This embossing method produced a much cleaner chip, with no sign of air bubbles, however, some parts of the plastic were not embossed properly. This is due to

not enough force that is applied by the binder clips. Measuring the height of the two parallel channels at the tip of the needle produced the same graph as Figure 5.5.

Method 7

The whole embossing assembly was changed to ensure that the force from the binder clips was applied to as much as the area as possible. Six 25 mm binder clips were used to apply as much force as possible, however, the larger glass slide would not allow these binder clips to reach the PDMS mould and COC hence, the glass slide that the PDMS mould was to be made was changed to a standard laboratory glass slide (Figure 5.7). The pressure applied to the embossing assembly was approximately 54 N

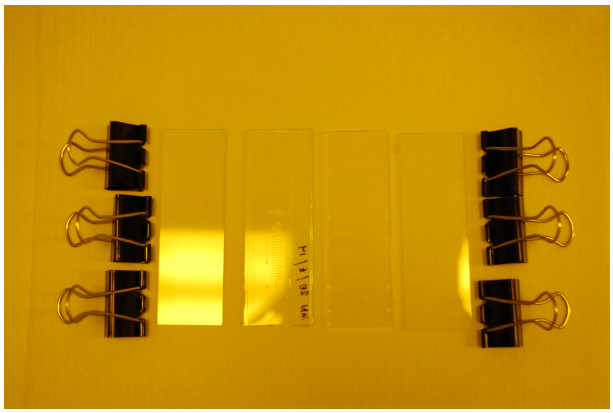

Figure 5.7: Components of the whole embossing assembly

The laboratory oven and the vacuum oven were preheated to 160°C and 180°C, respectively. The glass slides and a COC substrate were heated separately in the laboratory oven for 15 minutes to allow the COC substrate to commence reaching its glass transition temperature and the glass slide to retain the embossing assemblys temperature during the transfer between the laboratory oven and the vacuum oven. The assembly was placed into the vacuum oven for 25 minutes.

The resulting embossed slide contained almost no air bubbles on the channel side, however, there is an occurrence of cloudiness on the back side. During the preheating stage, the slide unexpectedly warped, which suggests that the preheating temperature was too high. When the slide channels were measured with the profiler, the graphs produced indicate that the embossing was perfect, with a channel height of 90 μm.

Method 8

After analysing each fabricated slide, it was noted that some of the air bubbles that appear after the embossing method is caused by dust particles that may be trapped

during assembly. To clean the slides, a cleaning method which is similar to cleaning methods used in photolithography was developed.

The glass slides were cleaned with acetone and washed with detergent and water. The COC slide was washed with isopropanol and water. All washed components were then dried with nitrogen gas. Similar to Method 7, the vacuum oven and laboratory oven were preheated to 180°C and 155°C respectively. To remove any left-over moisture that may be on the slides, the glass slides and the COC substrate were placed in the laboratory oven for 15 minutes. The embossing tool was assembled like in Method 7 and were placed in the vacuum oven for 25 minutes and allowed to cool to room temperature.

The height of the channel was measured to be 74 μm, however, the back side of the slide still have cloudy areas.

Method 9 and 10

The cleaning method from Method 8 had been adjusted to washing both the glass slides and the COC substrate with detergent and water in a 1:10 volume/volume ratio and placing them into an ultrasound machine. The laboratory oven was preheated to 90°C and the vacuum oven was preheated to 170°C where the glass slides and the COC substrate were preheated in the laboratory oven for 10 minutes. This produced a well-defined microfluidic channel, with the middle part of the cross-section at the same level as the substrate plane, however, the back side of the COC substrate contained multiple cloudly areas. The height of this channel was approximately 96 μm. The following methods were performed to find the parameters needed to prevent the cloudiness from appearing on the slide.

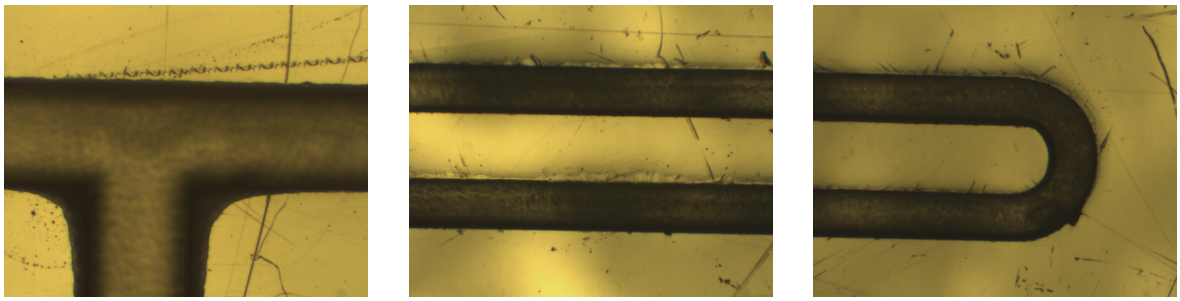

(a) T Junction **(b)** Channels **(c)** Tip

Figure 5.8: Resulting images of the device using Method 9

The difference between Method 9 (Figure 5.8) and Method 10 (Figure 5.9) is that Method 10 did not include the preheat and cooling steps, which consequentially shows the difference between the two.

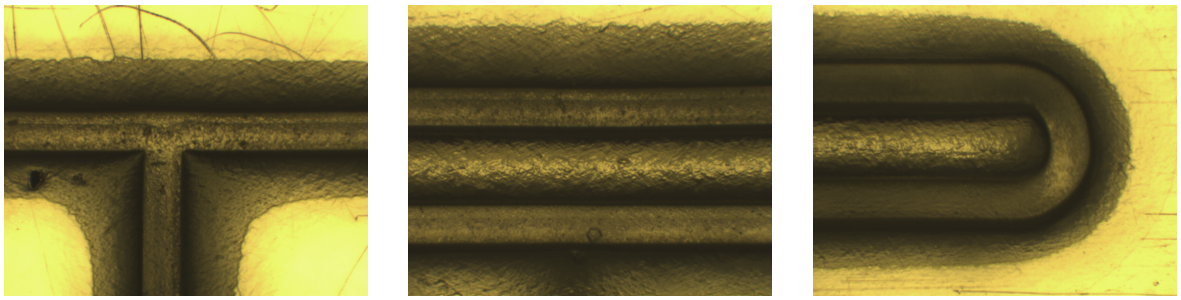

(a) T Junction **(b)** Channels **(c)** Tip

Figure 5.9: Resulting images of the device using Method 10

Method 11, 12, 13, and 14

It was observed that the vacuum oven takes an extended amount of time to reach the required temperature, and to stabilise at a constant temperature, hence an experiment was developed to observe if the embossing method is improved by leaving the embossing assembly in the vacuum oven for much longer.

The glass slides, the COC substrate, and the PDMS mould were washed and cleaned with detergent and water. They were then cleaned further in ultrasound in two mixtures:

- Detergent and water mixture in a 1:10 volume/volume ratio for 5 minutes
- Distilled water for 5 minutes

Each washed component were dried with nitrogen gas. The resulting embossed slides for each method were measured with the profiler and the graph shows that the cross-section of the channels were similar to what Figure 5.5 shows. This indicates that the time that the emboss assembly was left in the oven was too long according to the temperature of the oven.

Method 15

The glass slides, COC substrate and the PDMS mould were cleaned in ultrasound using the same process as Method 11. The emboss assembly was left in the vacuum oven for 15 minutes. The resulting slide was viewed under a microscope which showed that the channels were not embossed properly, suggesting that the channel height is less than 50um.

For this specific method, the height of the channel suggests that the emboss time was too short, not allowing the COC substrate to properly melt and let the PDMS mould to mould into the substrate.

Conclusion of the Embossing Method

Compared to previous embossed channels, Method 9 is considered to be the best method because the embossed channels look much sharper around the edges, and when the channels were measured using the profiler, the middle section is now at the same level as the substrate plane, as shown in Figures 5.8a, 5.8b and 5.8c.

5.1.4 Testing Embossing Channel

An experiment was done to test the embossed channels capability to act as a microfluidic channel, without the fluid leaking when lidded. Holes were drilled through the slide where the continuous and disperse phase ports are made, to enable injecting fluid into the channel. The slide was washed and lidded with adhesive tape. To make fluid flow into the microfluidic channel, a computerised fluid flow instrument (Fluigent Maesflow™) and an inverted epifluorescent microscope were used.

The first experiment involves seeing if fluid successfully flows through each channel normally. The fluid used in the aqueous channel is a Phosphate Buffered Saline (PBS) solution containing a fluorescent dye, fluorescein. This fluorescein will look fluorescent when exposed under blue light. Figure 5.10 shows that the fluid successfully flows through the microfluidic channel without leaking through the adhesive tape. The adhesive tape used is 9795R microtiter plate cover (Thermofisher Scientific©).

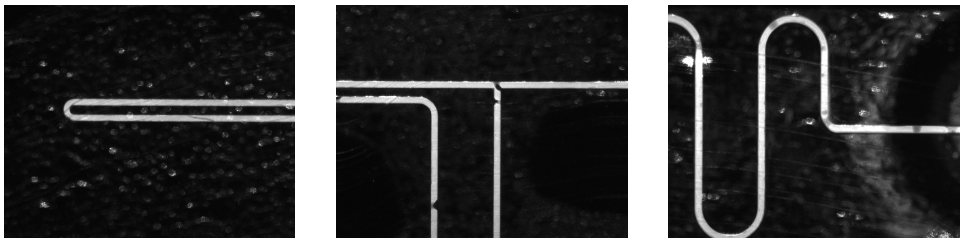

(a) Tip **(b)** T Junction **(c)** Fluid port

Figure 5.10: Images of different parts of the channel with fluoroscene mixture flowing through

A second experiment was done to see if the embossed channel is able to produce water droplets within the continuous oil phase. The disperse phase contains the same fluoroscine-water mixture as the first experiment. The continuous phase contains Fomblin 25/6 vacuum oil [9].

To create the droplets, the pressure applied to the oil channel is constant throughout the process at 200 $mbar$ (20 kPa). The water droplet generation is only reliant on changing the pressure of the water channel. Initially, the pressure applied to the water channel was

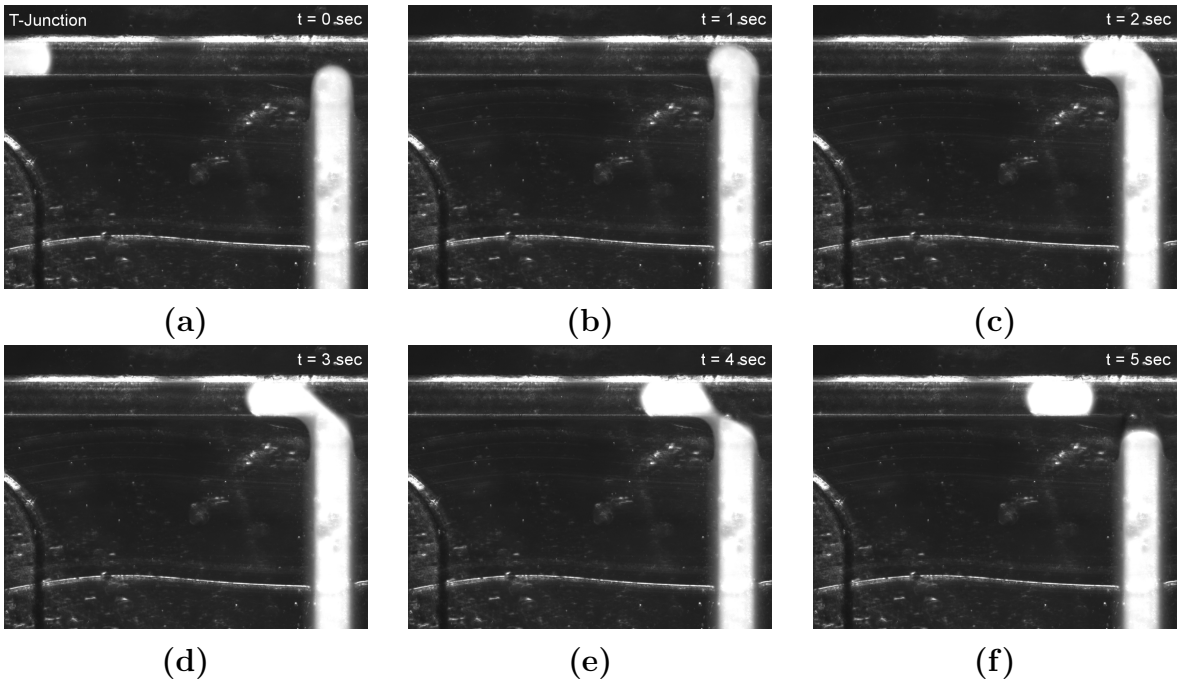

Figure 5.11: Sequence of droplet production at the T-junction of embossed channel

175 *mbar* (17.5 *kPa*) to bring the water level to the T-junction. The pressure is then increased to 190 *mbar* (19 *kPa*) for three seconds, and dropped to 180 *mbar* (18 *kPa*) to pull back the water level to finally finish the creation of the droplet.

Figure 5.11 illustrates the sequential images taken by a camera attached to the microscope. From these images, it shows that the embossed channel successfully creates water-in-oil droplets.

5.1.5 Conclusion

An embossing method to replicate a 100 $\mu m \times 100\ \mu m$ microfluidic channel in COC substrates was developed in Method 9. This involves cleaning every component with a detergent and water mixture, preheating the COC substrate to 90°C, applying a pressure of 54 *N* and placing the whole assembly into a vacuum oven at 170°C for 25 minutes. The effectiveness of this method is by running fluid into the channel and producing water droplets into the continuous oil phase, which is one of the main outcomes of the project.

The device has yet to achieve the temporal resolution of producing droplets within milliseconds. Figure 5.11 shows that a single droplet is formed within five seconds. This may be due to the pressure applied to both channels not allowing fast generation of droplets.

5.2 Bonding COC Substrates and Membranes

After testing that the microfluidic channel can form water droplets when the channel is lidded with an adhesive plastic, a COC lid is to be bonded to the substrate which contains the embossed microfluidic channel. To finally complete the prototype needle, a membrane is to be bonded to the COC lid according to the microfluidic channel design in Section 4.1. Using the bonding method found from bonding two COC substrates together, the COC lid, containing the bonded membrane will then be bonded to an embossed COC slide.

5.2.1 Experimental Aims

This experiment aims to develop the methods of bonding two COC substrates together, and a hydrophilic membrane to a COC substrate. A simple test to see if each bonding method works is to see if the two bonded materials will not come apart with moderate force applied by hand. The quality of the bond can also easily be observed by eye through the observation, or lack of, Newtons rings or interference fringes.

5.2.2 Methods

Bonding COC Substrates

Before applying a COC lid to the microfluidic channel, different methods of bonding were tested to see which method produces a proper seal for the channel. This seal will need to prevent any fluid that is running through the channel to flow outside of it. Similar to the embossing process, this experiment was iterative, to find the most optimised parameters.

Each component of the bonding method is placed in a bath containing a 10:1 water-detergent ratio mixture, and placed under ultrasound for 5 minutes. The components are dried with nitrogen gas and is finally assembled.

The bonding tool is assembled similarly to the embossing tool, however, the PDMS mould is replaced by a second COC substrate. The method of bonding relies on heating the COC to its glass transition temperature and using pressure on top of glass slides to make sure that the melted parts of the COC bond together on flat plane. The bonding tool was placed in a vacuum oven to apply heat and to prevent air bubbles from entering the bonding tool.

Each method iteration has been done at different temperatures, and different bonding environments as shown in Table 5.2.

Method No.	Temperature (°C)	Time (Minutes)
1	165-170	25
2	178	15
3	160-165	15
4	153	15

Table 5.2: Iterations of the bonding method

Bonding Membranes to COC Substrate

Another part of the bonding method is to bond a membrane from a filter unit (Sartorius Stedim Biotech©), to a COC substrate. The membrane itself contains microscopic pores that are 0.2 μm in diameter and is made from surfactant-free cellulose acetate (SFCA) [28]. Each membrane were cut into various shapes and sizes, including the size and shape that is intended to be used for the final bonding. The main iteration tests involve half-cut COC substrates that contains 0.5 mm drilled holes.

To bond the membrane, a bonding machine was used (Tresky T-3000-FC3™) (Figure 5.12). The machine contained a vacuum nozzle to pick and place samples onto a hotplate, which is controlled by a heater control. This machine is used as a die bonder and a component placer. Bonding typically requires the use of the installed hot plate. Component placing is performed by the pick and place tool, which contains a vacuum to pick up small components. The force measured by the tool is in grams-force.

The COC substrate is placed onto the hotplate to temperature, according to the method iteration and the membrane is picked up using vacuum and placed on top of the COC substrate. Typically, the COC substrate should be heated to its glass transition temperature to be able to bond materials to it. Similar to the bonding method, pressure is applied to the membrane. The machine contains a pressure sensor that monitors the pressure applied by the pick-up tool.

The process of bonding involves applying pressure on the edges of the membrane to the COC substrate, which is repeated until every part of the edge is bonded. The force applied for the first method was approximately 65 grams (0.64 Newtons), however, this was changed to 54 grams (0.53 Newtons), because applying 65 grams of force onto a COC substrate, heated to its glass transition temperature, will warp the substrate. The amount of time taken to apply the force to each area of the membrane was two minutes. Finding the temperature that is suitable for membrane bonding depends on the quality of the substrate when the bonding process is finished. If the temperature of the hot plate is too hot for the plastic, the heated parts of it will become foggy, and sometimes warp by itself.

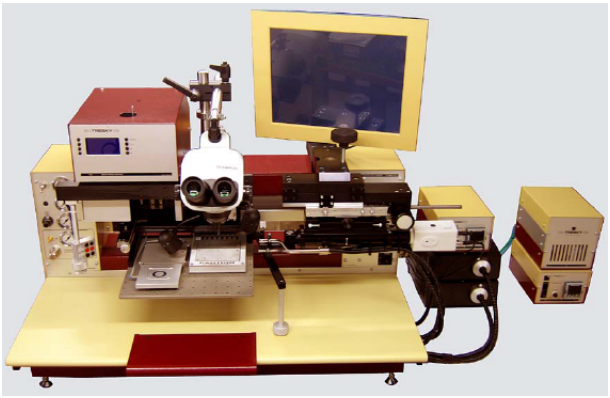

Figure 5.12: Tresky bonding machine

5.2.3 Results

Analysis was done for each bonded COC sample, however, each bonded sample contained Newtons rings. Figure 5.13 shows a bonded sample of two full-sized COC slides. Newtons rings is a phenomenon where light is refracted by the two bonded materials because both slides were not perfectly flat to each other when bonded, suggesting that air would have been trapped between both slides. After bonding a membrane to a COC slide, concentric to the drilled hole, a second COC piece was bonded to the first COC piece to trap the bonded membrane between the two slides (Figure 5.14).

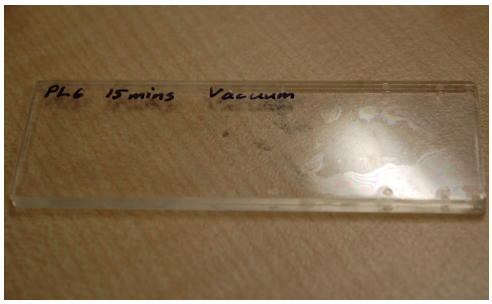

Figure 5.13: Bonded sample containing two COC substrates. The reflection of light highlights the Newton's rings

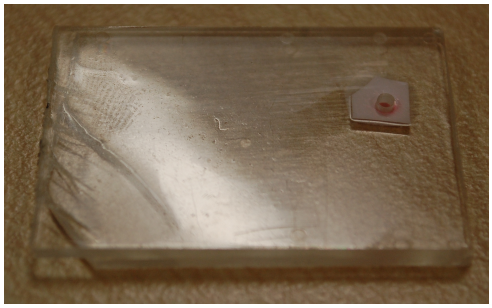

Figure 5.14: Sample containing a membrane bonded between two COC pieces

The bonded sample, containing the bonded membrane, is tested by injecting dyed water into the hole where the membrane is bonded, via the same chuck used for testing microfluidic flow in the embossed chip. Before being able to flow through the membrane, the water needs to wet the whole membrane. After wetting the membrane, the dyed fluid successfully flows through the membrane.

5.2.4 Conclusion

The bonding method that was found shows that the temperature needed to bond COC pieces together is much lower than what the embossing method needed. The method that produces the best bonded sample is placing the bonding tool inside the vacuum oven for 15 minutes at 153°C because the COC slides still contains a clear appearance after the bonding method.

Chapter 6

Conclusions and Future Work

6.1 Conclusions

This project shows that fabrication of a microfluidic channel in a COC, using binder clips as the source of the force of pressure still etches well-defined microfluidic channels. Most of the embossing methods produced incomplete channels, not well-defined channels. The incomplete channels occurred mainly in the first couple of iterations, which can be solved by adding more binder clips to the embossing assembly to provide more pressure, and increasing the temperature. The appearance of not well-defined channels could have been caused by leaving the embossing temperature too high, hence, lower levels were used.

The embossed channel, lidded with an adhesive tape was tested under the confocal microscope and the Maesflow system and it was able to form water droplets in a continuous oil phase.

The resulting bonded sample which contains a bonded membrane was able to let water droplets through it, even though it was bonded between two COC pieces. The membrane was able to stay in place at the output port even though it was completely wet.

During the course of the project, milestones were achieved, including finding methods to fabricate a well-defined microfluidic channel and bond hydrophilic membranes to COC substrates. The difficult part of the project was that very little information was found for embossing and bonding for the particular grade of COC, because different grades contains different physical properties, however, the method of repeating the experiment allows us to narrow down the optimal environment needed to emboss or bond to COC substrates.

6.2 Future Work

The bonding method only involves finding the parameters needed to bond a COC substrate and lid together, and bonding a membrane to a COC piece. Further developments will be done to bond a membrane to a lid, which contains the ports needed for inserting the oil and water into the system, and the output hole where water droplets will finally go through.

This lid will then be bonded to an embossed COC substrate, which will be tested with the confocal microscope and the Maesflow system to test if water droplets will successfully travel to the tip of the needle to be expelled through the hydrophilic membrane. The prototype needle will also to be tested if it can sample water droplets through the membrane, and through the microfluidic channels.

Future work will also include manufacturing the needle to its intended size, which will be tested by *in vivo* experiments. These experiments involves demonstrating droplet expulsion and collection in fake tissue made from agar.

Chapter 7

Abbreviations

ANFF-SA	Australian National Fabrication Facility at the University of South Australia
COC	Cyclic Olefin Colpolymer
CNC	Computer Numerical Control
CAD	Computer Aided Design
DBS	Deep Brain Stimulation
PDMS	Poly Dimethyl Siloxane
PMMA	Poly Methyl Methacrylate

Bibliography

[1] J. J. Bikerman, *Surface Chemistry: Theory and Applications*. Academic Press, Inc., 1958.

[2] A. Blackman, S. E. Bottle, S. Schmid, M. Mocerino, and U. Wille, *Chemistry*. John Wiley & Sons Australia Ltd, 2008.

[3] J. Brody, P. Yager, R. Goldstein, and R. Austin, "Biotechnology at low reynolds numbers." *Biophysical journal*, vol. 71, no. 6, pp. 3430–3441, 1996. [Online]. Available: http://dx.doi.org/10.1016/S0006-3495(96)79538-3

[4] H. Bruus, *Theoretical Microfluidics*. Oxford University Press, 2009.

[5] B. L. Carvalho, E. A. Schilling, N. Schmid, and G. J.Kellogg, "Soft embossing of microfluidic devices," *Miniaturized Chemical and Biochemical Analysis Systems*, 2003.

[6] D. Chen, W. Du, Y. Liu, W. Liu, A. Kuznetsov, F. Mendez, L. Philipson, and R. Ismagilov, "The chemistrode: a droplet-based microfluidic device for stimulation and recording with high temporal, spatial, and chemical resolution." *Proceedings of the National Academy of Sciences of the United States of America*, vol. 105, no. 44, pp. 16 843–16 848, 2008. [Online]. Available: http://dx.doi.org/10.1073/pnas.0807916105

[7] D. Collins, T. Alan, K. Helmerson, and A. Neild, "Surface acoustic waves for on-demand production of picoliter droplets and particle encapsulation." *Lab on a chip*, vol. 13, no. 16, pp. 3225–3231, 2013. [Online]. Available: http://dx.doi.org/10.1039/c3lc50372k

[8] R. Dangla, S. Kayi, and C. Baroud, "Droplet microfluidics driven by gradients of confinement." *Proceedings of the National Academy of Sciences of the United States of America*, vol. 110, no. 3, pp. 853–858, 2013. [Online]. Available: http://dx.doi.org/10.1073/pnas.1209186110

[9] Edwards, "H11312019 1 kg (529 ml)," 2012. [Online]. Available: http://www.edwardsvacuum.com/Products/H11312019/View.aspx

[10] C. P. Foley, N. Nishimura, K. B. Neeves, C. B. Schaffer, and W. L. Olbricht, "Flexible microfluidic devices supported by biodegradable insertion scaffolds for convection-enhanced neural drug delivery," *Biomedical microdevices*, vol. 11, no. 4, pp. 915–924, 2009. [Online]. Available: http://dx.doi.org/10.1007/s10544-009-9308-6

[11] A. Frohn and N. Roth, *Dynamics of Droplets*. Springer-Verlag, 2000.

[12] J. Galas, D. Bartolo, and V. Studer, "Active connectors for microfluidic drops on demand," *New Journal of Physics*, vol. 11, 2009. [Online]. Available: http://dx.doi.org/10.1088/1367-2630/11/7/075027

[13] V. N. Goral, Y. Hsieh, O. N. Petzold, R. A. Faris, and P. K. Yuen, "Hot embossing of plastic microfluidic devices using poly(dimethylsiloxane) molds," *Journal of Micromechanics and Microengineering*, vol. 21, 2011. [Online]. Available: http://dx.doi.org/10.1088/0960-1317/21/1/017002

[14] T. Kraus, E. Verpoorte, V. Liner, W. Franks, A. Hierlemann, F. Heer, S. Hafizovic, T. Fujii, N. F. de Rooij, and S. Koster, "Characterization of a microfluidic dispensing system for localised stimulation of cellular networks," *Lab on a Chip*, 2006. [Online]. Available: http://dx.doi.org/10.1039/B511768B

[15] T. Lomas, S. Mongpraneet, and A. Wisitsoraat, "Low cost hot embossing process for plastics microfluidic chips fabrication," *Electical Engineering/Electronics, Computer, Telecommunications and Information Technology*, 2009. [Online]. Available: http://dx.doi.org/10.1109/ECTICON.2009.5137048

[16] J. Narasimhan and I. Papautsky, "Polymer embossing tools for rapid prototyping of plastic microfluidic devices," *Journal of Micromechanics and Microengineering*, vol. 14, no. 1, 2004. [Online]. Available: http://dx.doi.org/10.1088/0960-1317/14/1/013

[17] T. Nisisako, T. Torii, and T. Higuchi, "Droplet formation in a microchannel network." *Lab on a chip*, vol. 2, no. 1, pp. 24–26, 2002. [Online]. Available: http://dx.doi.org/10.1039/b108740c

[18] D. Noonan, "Mind Craft," *Smithsonian*, vol. 45, no. 2, pp. 38–47, May 2014.

[19] J. J. Norman, J. M. Arya, M. A. McClain, P. M. Frew, M. I. Meltzer, and M. R. Prausnitz, "Microneedle patches: Usability and acceptability for self-vaccination against influenza," *Vaccine*, vol. 32, no. 16, pp. 1856–1862, 2014.

[20] E. Palermo, "Tiny Implants Could Give Humans Self-Healing Superpowers," September 2014. [Online]. Available: http://news.discovery.com/tech/biotechnology/tiny-implants-could-give-humans-self-healing-powers-140922.htm

[21] P. Patel, "Integrated Implant Makes It Easier to Control the Brain With Light," February 2013. [Online]. Available: http://spectrum.ieee.org/biomedical/diagnostics/integrated-implant-makes-it-easier-to-control-the-brain-with-light

[22] ——, "Electronic Skin Patch With Memory and Drug Delivery Capability Could Treat Parkinson's," March 2014. [Online]. Available: http://spectrum.ieee.org/tech-talk/biomedical/devices/electronic-skin-patch-with-memory-and-drug-delivery-could-treat-parkinsons

[23] ——, "New Eye Sensor Could Be Boon for Glaucoma Patients," August 2014. [Online]. Available: http://spectrum.ieee.org/tech-talk/biomedical/diagnostics/implanted-eye-sensor-with-smartphone-readout

[24] F. Pirmoradi, J. Jackson, H. Burt, and M. Chiao, "A magnetically controlled MEMS device for drug delivery: design, fabrication, and testing." *Lab on a chip*, vol. 11, no. 18, pp. 3072–3080, 2011. [Online]. Available: http://dx.doi.org/10.1039/c1lc20438f

[25] C. Pozrikdis, *Fluid Dynamics: Theory, Computation, and Numerical Simulation*. Springer Science+Business Media, 2009.

[26] R. Rathnasingham, D. Kipke, S. Bledsoe Jr., and J. McLaren, "Characterization of implantable microfabricated fluid delivery devices," *IEEE Transactions on Biomedical Engineering*, vol. 51, no. 1, pp. 138–145, 2004. [Online]. Available: http://dx.doi.org/10.1109/TBME.2003.820311

[27] B. Rubehn, S. Wolff, P. Tovote, A. Lüthi, and T. Stieglitz, "A polymer-based neural microimplant for optogenetic applications: design and first in vivo study." *Lab on a chip*, vol. 13, no. 4, pp. 579–588, 2013. [Online]. Available: http://dx.doi.org/10.1039/c2lc40874k

[28] Sartorius, "Minisart®NML Syringe Filters 16534———-K," 2014. [Online]. Available: http://www.sartorius.com/en/product/product-detail/16534-k/

[29] D. J. Shaw, *Introduction to Colloid and Surface Chemistry*, 3rd ed. Butterworth Pty Ltd, 1980.

[30] E. Strickland, ""Bionic Eye" Implants Will Hit the U.S. Market This Year," February 2013. [Online]. Available: http://spectrum.ieee.org/tech-talk/biomedical/bionics/bionic-eye-implants-will-hit-the-us-market-this-year

[31] S. Teh, R. Lin, L. Hung, and A. Lee, "Droplet microfluidics," *Lab on a chip*, vol. 8, no. 2, pp. 198–220, 2008. [Online]. Available: http://dx.doi.org/10.1039/b715524g

[32] D. Tondeur, Y. Fan, J. Commenge, and L. Luo, "Flow and pressure distribution in linear discrete ladder-type fluidic circuits: An analytical approach," *Chemical Engineering Science*, vol. 66, 2011. [Online]. Available: http://dx.doi.org/10.1016/j.ces.2011.03.003

[33] J. Toon, "Self-Administration of Flu Vaccine with a Patch May be Feasible, Study Suggests," February 2014. [Online]. Available: http://www.news.gatech.edu/2014/02/26/self-administration-flu-vaccine-patch-may-be-feasible-study-suggests

[34] D. Tritton, *Physical Fluid Dynamics*. Van Nostrand Reinhold Company Ltd, 1979.